

RESEARCH

Open Access



Threshold estimation based on local minima for nucleus and cytoplasm segmentation

Simeon Mayala^{1*} and Jonas Bull Haugsøen^{2,3}

Abstract

Background: Image segmentation is the process of partitioning an image into separate objects or regions. It is an essential step in image processing to segment the regions of interest for further processing. We propose a method for segmenting the nuclei and cytoplasm from white blood cells (WBCs).

Methods: Initially, the method computes an initial value based on the minimum and maximum values of the input image. Then, a histogram of the input image is computed and approximated to obtain function values. The method searches for the first local maximum and local minimum from the approximated function values in the order of increasing of knots sequence. We approximate the required threshold from the first local minimum and the computed initial value based on defined conditions. The threshold is applied to the input image to binarize it, and then post-processing is performed to obtain the final segmented nucleus. We segment the whole WBC before segmenting the cytoplasm depending on the complexity of the objects in the image. For WBCs that are well separated from red blood cells (RBCs), n thresholds are generated and then produce n thresholded images. Then, a standard Otsu method is used to binarize the average of the produced images. Morphological operations are applied on the binarized image, and then a single-pixel point from the segmented nucleus is used to segment the WBC. For images in which RBCs touch the WBCs, we segment the whole WBC using SLIC and watershed methods. The cytoplasm is obtained by subtracting the segmented nucleus from the segmented WBC.

Results: The method is tested on two different public data sets and the results are compared to the state of art methods. The performance analysis shows that the proposed method segments the nucleus and cytoplasm well.

Conclusion: We propose a method for nucleus and cytoplasm segmentation based on the local minima of the approximated function values from the image's histogram. The method has demonstrated its utility in segmenting nuclei, WBCs, and cytoplasm, and the results are satisfactory.

Keywords: Segmentation, Local minima, Nucleus and cytoplasm

Background

White blood cells (WBCs) are cells of the immune system that take part in the body's defense against infectious disease and foreign material [1, 2]. WBCs can be categorized based on structure (granulocytes or agranulocytes) and cell lineage (myeloid or lymphoid cells). Broadly, there are

five types of WBCs; three types of granulocytes—neutrophils, eosinophils, and basophils, and two types of agranulocytes—lymphocytes and monocytes. Granulocytes and monocytes are of myeloid lineage, whereas lymphocytes are, as the name implies, of lymphoid lineage.

In microscopic images of stained blood smears, WBCs can be differentiated from red blood cells and platelets by having nuclei and their (in most cases) larger size. They also stain darker using common dyes such as hematoxylin and eosin (H&E). Three main characteristics are used

*Correspondence: simeon.mayala@uib.no

¹ Department of Mathematics, University of Bergen, Allégaten 41, 5007 Bergen, Norway

Full list of author information is available at the end of the article



to identify the different types of WBCs - the shape of their nuclei, their granularity, and their staining.

All the granulocytes are large, granular cells with lobulated nuclei [2]. Neutrophils stain neutrally and have nuclei with multiple (2–5) lobes. Eosinophils stain red and have nuclei with 2–4 lobes. Basophils stain blue and have nuclei with 2–3 lobes. The shapes of these lobes are characteristic for each cell type, as seen in Fig. 1. Monocytes are large agranular cells with kidney-shaped nuclei. Lymphocytes are also agranular and are smaller than the other WBCs. Their nuclei are round, often eccentric, and stain dark blue. Examples of the different types of WBCs can be seen in Fig. 1.

Image segmentation is a process that separates a region of interest (ROI) from the background to simplify further analysis [3, 4]. Different methods for segmenting images have been developed. They are classified differently based on how they perform the segmentation. Example of the popular methods include thresholding [5–9], edge detection [10], morphologically based [11], graph based [12–14], clustering based [15], watershed [16], level-set based [17] and a combination of different methods [2, 18–20]. Convolutional neural networks (CNN) are deep learning techniques and they have been widely used for WBCs segmentation [21–23]. We review related literature concerning WBC and nucleus segmentation.

Mittal et al. [24] presents a comprehensive review of different computer-aided methods for analyzing blood smear images and leukemia detection. The paper reviews 149 papers by presenting different techniques used for preprocessing images and WBC segmentation methods. It provides different workflow pipelines for segmenting WBC based on knowledge, deformable models, and machine learning. Also, the review gives the merits and demerits of each method.

Li et al. [9] proposed a dual-threshold method for segmenting WBC based on a strategic combination of the RGB and HSV colour spaces by searching for an optimal threshold using a golden section search method. Ghane et al. [18], proposed a method for segmenting WBC

based on a combination of thresholding, K-means clustering and a modified watershed algorithm. Also, Kuse et al. [19] proposed a method that segments cells using mean shift-based clustering for color approximation and then thresholding. Features are extracted and then used to train a support vector machine (SVM) classifier for classifying lymphocytes and non-lymphocytes. Prinyakupt et al. [2] proposed a system that pre-processes the images by locating the WBCs and then segmenting them into nucleus and cytoplasm.

Theera-Umpon [11] proposed a method that uses a fuzzy C-means (FCM) algorithm and mathematical morphological operations to segment WBCs. Miao and Xiao [16] proposed a marker-controlled watershed algorithm for segmenting WBCs and RBCs. Yung-Kuan et al. [10] propose a method for WBC nucleus segmentation and counting the lobes in a nucleus that works by object contour detection. Furthermore, Salem [15] proposed a WBC segmentation method based on the K-means clustering technique. The method converts RGB to the $L * a * b$ color space and then the a and b components are used as features in the clustering algorithm. Sadeghian et al. [20] propose a framework that integrates several digital image processing algorithms for segmenting nucleus and cytoplasm. Khamael et al. [17] propose a method for the segmenting nuclei of WBC from the cytoplasm and the cell wall. The method performs segmentation based on level set methods and geometric active contours.

Banik et al. [21] proposed a method that segments WBC nuclei based on a $L * a * b$ color space conversion and K-means algorithm. Then, WBCs are located using the segmented nucleus. A convolutional neural network (CNN) is used to classify the localized WBC image. Fan et al. [22] proposed a method for localization and segmentation of WBCs. The method uses pixel-level information for training a deep convolutional neural network to locate and segment the region of interest. Lu et al. [23] proposed a WBC-NET based on the UNet++ and ResNet to improve the accuracy of the

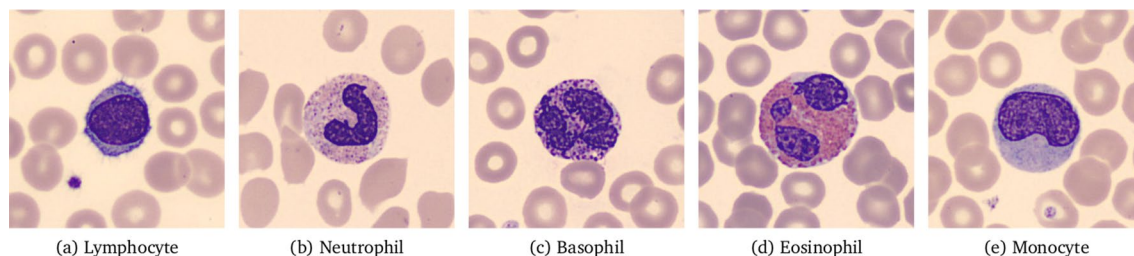


Fig. 1 Normal white blood cells. The cells seen in the background are red blood cells identified by their red color, thin (often almost transparent) center, and lack of nuclei

WBCs segmentation. Furthermore, Long [25] proposed an enhanced, light-weighted U-Net with a modified encoded branch. The method explores the possibility of performance improvement of cell nucleus segmentation algorithms through deep learning, requiring less pre-and post-processing of images.

Our contribution in this work concerns the way the method estimates the threshold. A histogram of the input image is computed, and the function values are approximated. The threshold is estimated based on the local minima of the approximated function values. The estimated threshold is applied to the input image to segment the nucleus. Also, we develop a simple strategy for segmenting the WBC whenever is well separated from surrounding red blood cells. We generated n different thresholds and each threshold is applied to the input image to produce n thresholded images. The produced images are combined by taking their average and then a standard Otsu method is used to binarize it. We perform post-processing and use a single-pixel point from the nucleus to extract the WBC. The cytoplasm is obtained by subtracting the segmented nucleus from the segmented WBCs.

For images whose WBCs touch RBCs, we opt for classical techniques to separate the touching objects. We use the Simple Linear Iterative Clustering (SLIC) approach based on superpixels [26]. Since the focus is on the WBCs, we utilize the superpixel’s strength of boundary adherence to segment the WBCs. We also apply a

watershed transformation to segment the WBC [27]. The number of local maxima is chosen automatically. When the WBC is detached from the uninteresting objects, we perform post-processing so that only the WBC remains.

Methods

In this section, we establish a method for segmenting the nucleus and cytoplasm based on the distribution of the intensity values of the input image. The technique estimates the threshold automatically based on the local minima of the estimated function values. The summarized steps for nucleus, WBC, and cytoplasm segmentation are visualized in Fig. 2.

Threshold estimation for nucleus segmentation

Assuming that a gray-scale image has intensity values that can be classified into several gray levels. Let a gray-scale image A be a matrix of $M \times N$ dimension such that $f(x, y)$ gives an intensity value at position (x, y) . We define,

$$A = [f(x, y)]_{M \times N} \text{ for } x = 0, 1, \dots, N - 1; y = 0, 1, \dots, M - 1 \tag{1}$$

Considering the input image A in Eq. 1, we compute a value T_{nc0} that will be used to search for a threshold value for segmenting the nucleus. The T_{nc0} value is computed from the input image by

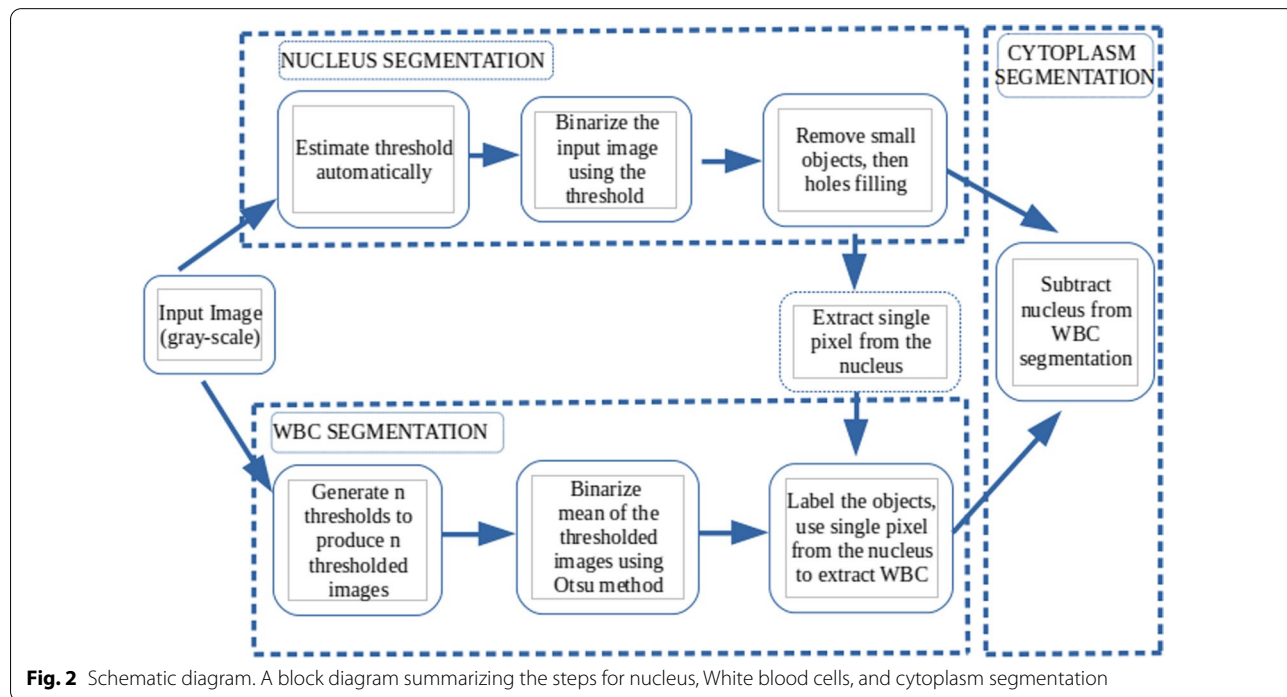


Fig. 2 Schematic diagram. A block diagram summarizing the steps for nucleus, White blood cells, and cytoplasm segmentation

$$T_{nc0}(n_1, n_2) = \frac{Max(A)}{n_1} + \frac{Min(A)}{n_2} \tag{2}$$

Where n_1 and n_2 are integers greater than 0. A simple analysis on how to choose n_1 and n_2 is presented in Additional file 1. Assuming that T_{nc0} is an intensity value on the histogram of the input image A . We want to estimate T_{nc0} such that $Min(A) < T_{nc0} < Max(A)$. We represent the input image A in a form that increases monotonically to locate the value T_{nc0} . Let \tilde{A} be a vectorized matrix of A , then the intensity values $f(x, y)$ at each position (x, y) in the vectorized matrix are

$$\tilde{A} = [f(x, y)_0, f(x, y)_1, f(x, y)_2, \dots, f(x, y)_{k-2}, f(x, y)_{k-1}]^T \tag{3}$$

Where k is the total number of pixels in the image A and T is a transpose. We construct a non-decreasing sequence of values in \tilde{A} by using the intensity values $f(x, y)$ at each position in \tilde{A} . Then, the sequence will be

$$\tilde{A}_{seq} = [f(x, y)_i \leq f(x, y)_{i+1} \leq \dots \leq f(x, y)_{k-2} \leq f(x, y)_{k-1}] \tag{4}$$

The constructed sequence of intensity values in \tilde{A}_{seq} are ordered sets and preserve a non-decreasing order, so it takes the form of a monotonically increasing function. For each $f(x, y) \in \tilde{A}_{seq}$ we can write $f(x, y)_i \rightarrow I_i$. The form has been changed from the function of two variables $f(x, y)$ in image A into the function of one variable in \tilde{A}_{seq}

$$\tilde{A}_{seq} = [I_i \leq I_{i+1} \leq \dots \leq I_{k-2} \leq I_{k-1}] = [I_i, \dots, T_{nc0}, \dots, I_{k-1}] \tag{5}$$

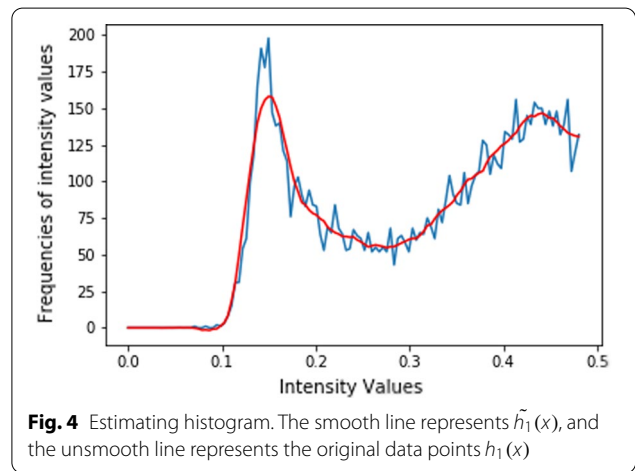
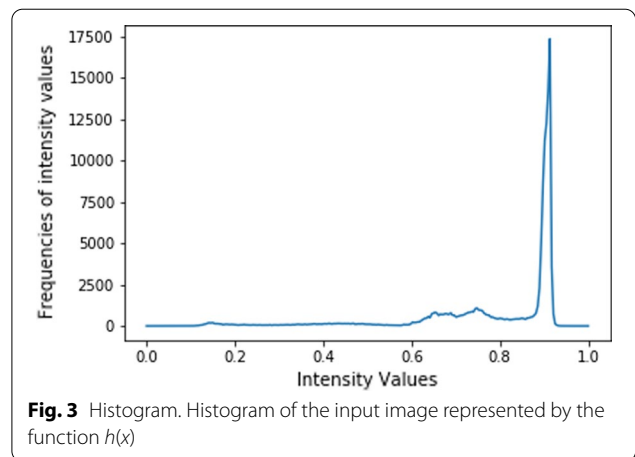
T_{nc0} is not necessarily one of the values in \tilde{A}_{seq} but it is within the range of \tilde{A}_{seq} . A threshold $\tilde{\epsilon}_t$ will be estimated after representing the intensity values of the input image in the form of a histogram. T_{nc0} together with some conditions will be used to approximate the required threshold value.

Approximating threshold $\tilde{\epsilon}_t$

Let $h(x)$ be the function representing the histogram of an image A , where x is an intensity value I , and $h(x)$ is the frequency of the intensity values (see Fig. 3). Let $\tilde{h}(x)$ be the approximation of $h(x)$ (see Fig. 4). We approximate $h(x)$ without distorting the general tendency of the histogram function. We can decompose $\tilde{h}(x)$ into

$$\tilde{h}(x) = \tilde{h}_1(x) + \tilde{h}_2(x) \tag{6}$$

Let $(x_i, \tilde{h}_1(x_i))_{i=1}^m$ be the given points from the approximated histogram. We need to compute a spline g such that

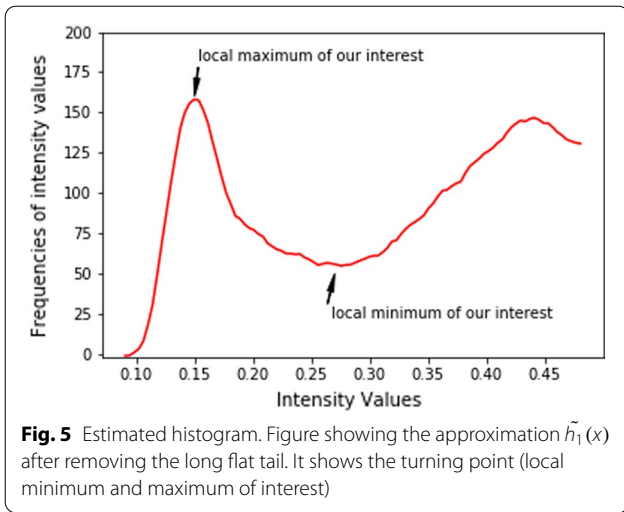


$$g(x_i) = \tilde{h}_1(x_i), \text{ for } i = 1, \dots, m \tag{7}$$

The spline concept and basis spline (B-spline) is presented in Additional file 1 [28, 29]. Assuming that the spline is smooth and we are interested in the number of turning points produced from the spline $g(x)$. We utilize the local propagation of B-Spline to choose any degree we want. So, a $g(x)$ polynomial of n degrees gives $n - 1$ turning points. Setting d be the degree of $g(x)$, the turning points will be $(x_1, g(x_1)), (x_2, g(x_2)), \dots, (x_{d-1}, g(x_{d-1}))$.

Let $(x_c, g(x_c)), (x_{c+1}, g(x_{c+1}))$ be first local maximum and minimum of the function $g(x)$ respectively. Based on the filtered data points of Fig. 5, the threshold $\tilde{\epsilon}_t$ is expected to be closer to the first local minimum of the function $g(x)$. Also, the threshold $\tilde{\epsilon}_t$ must appear after the first local maximum of the function $g(x)$ in the order of increase of the knots.

Also, from Eq. 2, the sensitivity analysis of T_{nc0} in the Additional file 1 guarantees that the value of T_{nc0} will not



be very far from $\frac{1}{3}$. We introduce a parameter Er which is a small value chosen to control T_{c0} and the local minimum value during threshold estimation. Then, the threshold $\tilde{\epsilon}_t$ is computed by checking the following conditions:

- (a) $x_c < T_{nc0}$.
- (b) If $|T_{nc0} - x_{c+1}| < Er$ then, $\tilde{\epsilon}_t = \frac{T_{nc0} + x_{c+1}}{2}$.
- (c) If $|T_{nc0} - x_{c+1}| > Er$ and $T_{nc0} > x_{c+1}$ then, $\tilde{\epsilon}_t = \frac{T_{nc0} + x_{c+1} + Er}{2}$.
- (d) If $|T_{nc0} - x_{c+1}| > Er$ and $T_{nc0} < x_{c+1}$ then, $\tilde{\epsilon}_t = \frac{T_{nc0} + x_{c+1} - Er}{2}$.

The threshold $\tilde{\epsilon}_t$ is applied on the input image A to produce image A_{recons} . We call it a reconstructed image, and it is mathematically obtained by

$$A_{recons} = \begin{cases} \text{Min}(A) & \text{if } f(x, y) \leq \tilde{\epsilon}_t \\ f(x, y) & \text{elsewhere} \end{cases}$$

The image A_{recons} is binarized to segment the nucleus of the WBCs. Then, post-processing operations are applied to the binarized image to obtain the final segmented nucleus.

Threshold estimation for WBC segmentation

We develop a strategy for segmenting the WBC after pre-processing the input image. The input image is pre-processed by averaging n thresholded images of the input image to reduce the variability of intensity values in the WBC region. The n images are obtained using different thresholds produced in a defined range by using

$$T_{wbc}^i = \frac{\text{Max}(A) + T_{nc0}}{2} + er_i \quad (8)$$

where er_i is a step size between consecutive thresholds in a defined interval, $i = 0, 1, 2, \dots, n - 1$.

Let a_l and a_u be lower and upper limit of the intensity values in the chosen interval respectively. We denote er_i by Δh . Then, Δh is a step size between two consecutive thresholds T_{wbc}^i and T_{wbc}^{i+1} in the interval between a_l and a_u . To generate n equal sub-intervals in the defined interval we use

$$n = \frac{a_u - a_l}{\Delta h} \quad (9)$$

as $\Delta h \rightarrow 0$, $n \rightarrow \infty$ and $(a_u - a_l)$ is fixed. T_{wbc}^i will be generated at the interval Δh . So, for the interval $a_l \leq er_i \leq a_u$ divided into $n - 1$ equal subintervals is represented as

$$a_l = T_{wbc}^0 < T_{wbc}^1 < T_{wbc}^2 < \dots < T_{wbc}^{n-1} = a_u \quad (10)$$

where $T_{wbc}^i = a_l + i \Delta h$, for $i = 0, 1, 2, \dots, n - 1$ and $\Delta h = \frac{a_u - a_l}{n}$. Each T_{wbc}^i is used to produce one thresholded image from the input image A by

$$A_j = \begin{cases} T_{wbc}^i & \text{if } f(x, y) \leq T_{wbc}^i \\ f(x, y) & \text{elsewhere} \end{cases} \quad (11)$$

Since i varies from 0 to $n - 1$, then the reconstructed (preprocessed) image for WBC is produced by

$$A_{wbc} = \frac{1}{n} \sum_{j=0}^{n-1} A_j \quad (12)$$

The image A_{wbc} reduces the contrast in the WBCs region and the plasma membrane of the RBCs. The image A_{wbc} is binarized to segment the WBCs from RBCs and other background. Note that the strategy works well for images whose WBCs are well separated from RBCs as well as the choice of n . For images whose WBCs touch the RBCs, we opt for classical techniques to segment the WBCs. The cytoplasm is obtained by subtracting the segmented nucleus from the segmented WBCs.

Descriptions of data

The proposed method is tested on two different WBC image datasets. The first image dataset contains a total of 17,092 images of individual normal cells, which were acquired using the analyzer CellaVision DM96 in the Core Laboratory at the Hospital Clinic of Barcelona [30]. The dataset is organized into eight different groups. It includes neutrophils, eosinophils, basophils, lymphocytes, monocytes, immature granulocytes, erythroblasts, and platelets (thrombocytes). It is a high-quality labeled dataset that can be used for benchmarking, training, and testing models. They are JPG images with a size of (360×363) pixels for each image. For more information refer to [30].

The second image dataset used in [31] contains 300 images together with the manually segmented images. The dataset was originally obtained from iangxi Tecom Science Corporation, China. The nuclei, cytoplasm, and background including red blood cells are marked in white, gray, and black respectively. The images were acquired using a Motic Moticam Pro 252A optical microscope camera with an N800-D motorized auto-focus microscope, and the blood smears were processed with a newly-developed hematology reagent for rapid WBC staining [31]. They are 120×120 images of WBCs.

Implementation and experimental results

Nucleus segmentation

The input images are converted into grayscale. For each grayscale image, a value T_{nc0} is computed using Eq. 4(a) in Additional file 1. Then, a *NumPy function histogram* is used for computing a histogram of the input image [32]. The histogram is decomposed into two equal parts and then run a script on the first part of decomposition to check and remove the long flat tail at the beginning (see Figs. 4 and 5). Then, a SciPy function *savgol filter* is applied to obtain the approximated function values [33]. A *B-spline* (3rd order polynomial) interpolation function is applied on the approximated function values and then the *argrelextrema* function is used to compute the local minima and maxima [33]. Note that if the local minima and maxima are not found in the first run, the length of decomposition is incremented, and start searching again until the first local maximum and minimum are found. The values of the first local maximum and minimum together with the value T_{nc0} are used for computing the threshold $\tilde{\epsilon}_t$ based on the conditions given in the methodology subsections. The threshold $\tilde{\epsilon}_t$ is applied on the input image to preprocess and binarize it to segment the nucleus. The binarized image is post-processed by applying a morphological operation to remove small objects and close holes if they exist. The result is the segmented nucleus of the input image. Some results for the implementation steps are visualized in Fig. 6.

WBC and cytoplasm segmentation

We generate n values automatically in the interval $[Min(A), \frac{Max(A)}{3}]$ which are referred as step size er_i in Eq. 8. For each value in the interval we compute threshold T_{wbc}^i using Eq. 8. Each threshold is applied to the input image to generate n thresholded images using Eq. 11. The n thresholded images are averaged using Eq. 12 to obtain a preprocessed image A_{wbc} and then binarize it using a standard Otsu thresholding method

[34]. Then, morphological operations are applied to separate the WBC from the background and RBCs. From the segmented nucleus (in the previous sub-section), we take a single pixel value location and use it to extract the whole WBC from the binarized image. The cytoplasm is obtained by subtracting the segmented nucleus from the WBC. Figure 7 visualizes some images summarizing the steps for nucleus and WBC segmentation.

For images whose WBCs touch the RBCs we opt for two classical approaches and use them to segment the WBCs.

We apply the Simple Linear Iterative Clustering (SLIC) approach based on superpixel [26, 35]. Since the superpixel algorithm adheres to boundaries, we focus on identifying the WBCs boundaries whenever the RBCs touch the WBCs. We allow under segmentation in order to segment well the WBCs. The results are visualized in Fig. 8 fifth column.

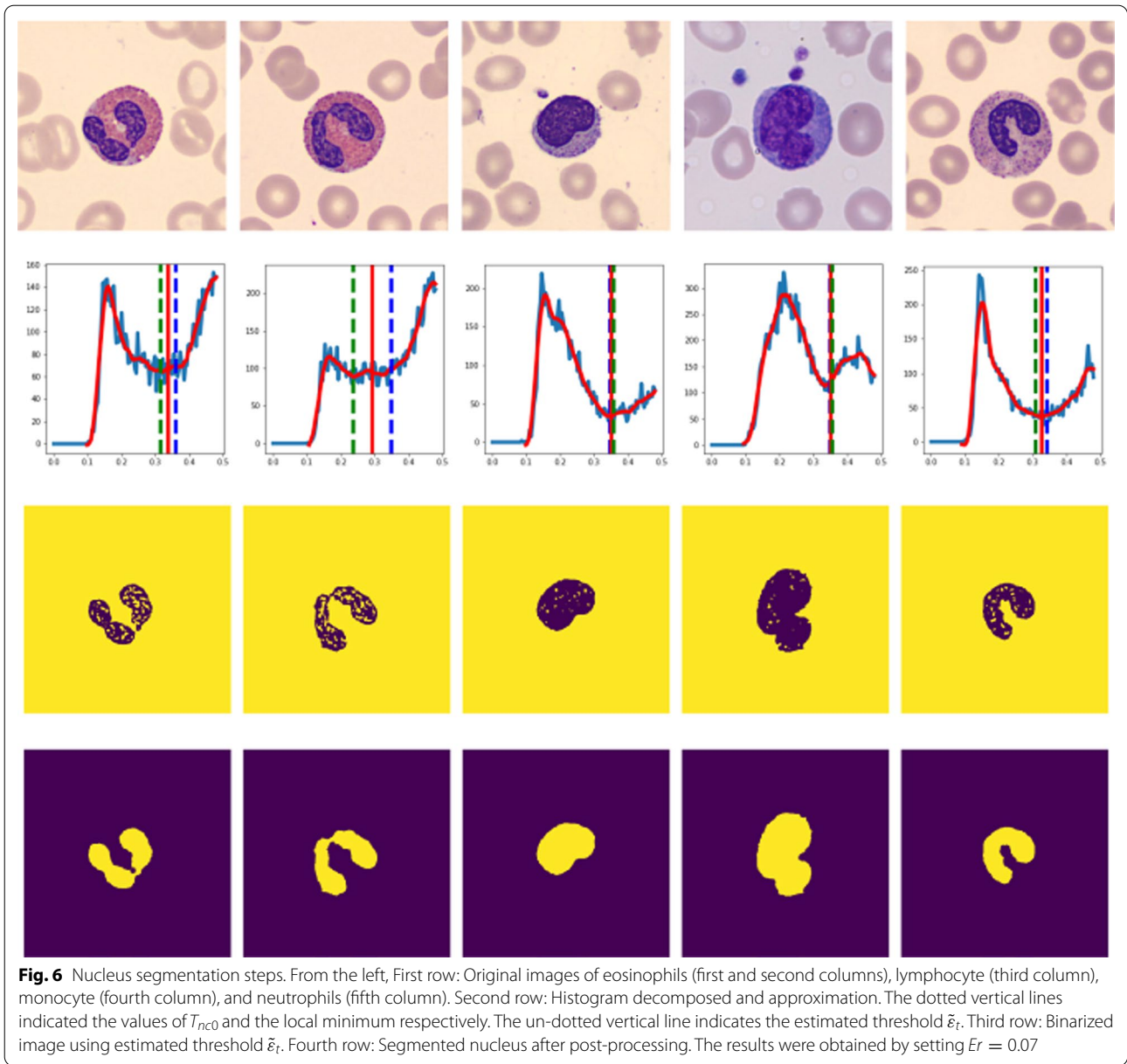
We also apply watershed transformation for segmenting the WBCs when the RBCs touch the WBCs. The approach is a transformation on grayscale images [27]. It aims at detaching the ROI from the non interesting objects when the edges of these objects touch each other. We concentrate on the marker construction step where it is easier to control it. We allow an automatic choice of the number of local maxima and retain the results if the RBCs are detached from the WBCs. In this step, we do not care much about the over-segmentation of the ROI, instead, we focus on detaching the uninteresting objects from the object of interest (the WBC). The results are visualized in Fig. 8 third column.

Note that the input for watershed can be either image gradient or binarized image. Both options work but the challenging part is to control the markers. Looking at Fig. 8 third column it could be challenging to identify the required labels and then remove the unwanted ones. Figure 8 fifth column shows that SLIC is straightforward because it identifies the boundaries of the WBCs.

Quantitative analysis

We present a simple analysis to assess the efficiency and effectiveness of the proposed method. The performance evaluation is done by a quantitative measure of the segmentation results. We analyze the accuracy by evaluating the similarity between the segmentation results obtained using the proposed method and the ground truth.

We compute Jaccard Index (JI), Dice similarity coefficients (DSC), Sensitivity, Specificity, and Precision to check the level of similarity between the ground truth and the segmentation from the proposed method (predicted segmentation). The Jaccard Index (J) is defined by



$$J(L_M, L_P) = \frac{|L_M(x, y) \cap L_P(x, y)|}{|L_M(x, y) \cup L_P(x, y)|} = \frac{TP}{TP + FP + FN} \quad (13)$$

where $|L_M(x, y)|$ is the number of labels in the ROI from the ground truth. $|L_P(x, y)|$ is the number of labels in ROI obtained using the proposed method. $|L_M(x, y) \cap L_P(x, y)|$ is the number of labels appearing in the ROI from the ground truth and the predicted segmentation. The Dice Similarity Coefficient is defined by

$$DSC(L_M, L_P) = \frac{2|L_M(x, y) \cap L_P(x, y)|}{|L_M(x, y)| + |L_P(x, y)|} = \frac{2TP}{2TP + FP + FN} \quad (14)$$

We can also use the concept of true positive (TP), false positive (FP), true negative (TN), and false-negative (FN) to check the performance of the method. We compute Sensitivity, Specificity, and Precision as follows.

$$\begin{aligned} Sensitivity &= \frac{TP}{TP + FN}, \quad Specificity \\ &= \frac{TN}{TN + FP}, \quad Precision = \frac{TP}{TP + FP} \end{aligned} \quad (15)$$

In the quantitative analysis we use the second data set used in [31] because the first data set in [30] does not have the ground truth images. In the analysis, some

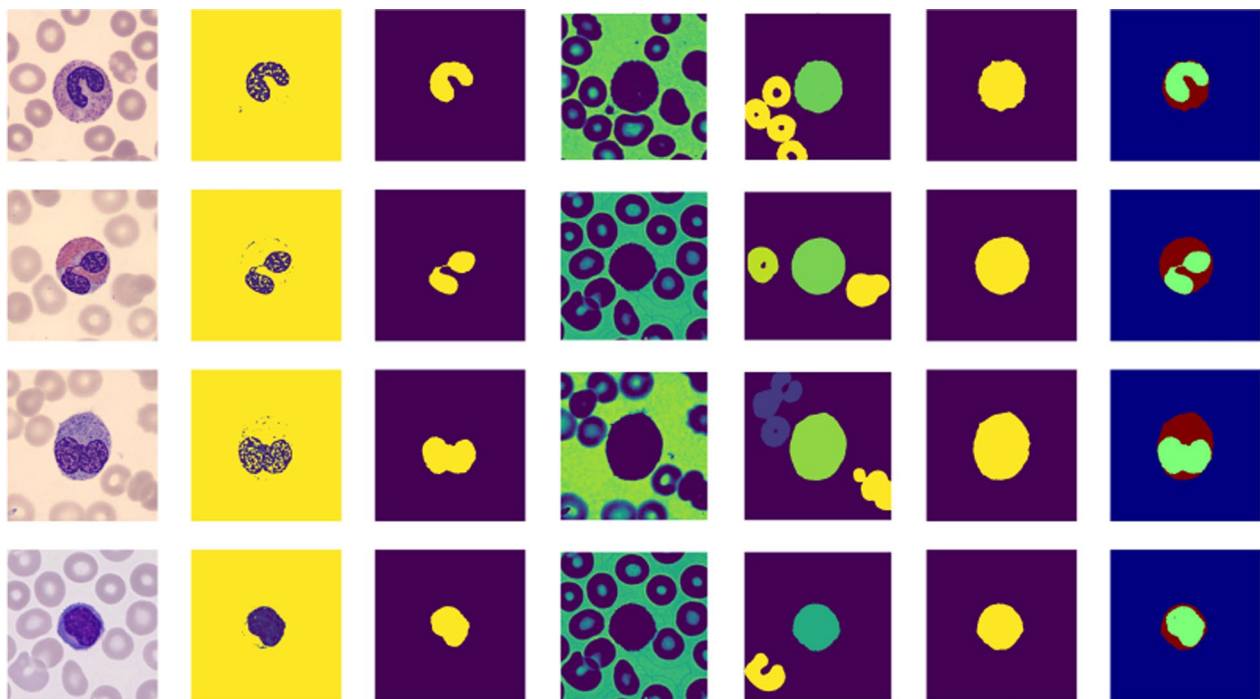


Fig. 7 WBC and cytoplasm segmentation steps. From the left, First column: input images, Second column: Reconstructed images and then binarized using estimated threshold $\tilde{\epsilon}_t$ for nucleus segmentation. Third column: Segmented nucleus after post-processing. Fourth column: Reconstructed images after averaging different thresholded images. Fifth column: Assigning new labels to the objects and removing some objects. Sixth column: Segmented WBC using a single-pixel value location from the segmented nucleus. Seventh column: Segmented nucleus and cytoplasm. From top to down: the first row is the neutrophil, the second row is the eosinophil, the third row is the monocyte, the fourth row is the lymphocytes

images were not included because of different reasons. Some of the images not considered in this section include the ones visualized in Fig. 9 showing the original and the ground truth,

A quantitative evaluation was performed by comparing the level of similarity between the ground truth and the segmentation obtained using the proposed method. The JI, DSC, Sensitivity, Specificity, and precision metrics range from 0 to 1. Zero indicates that there is no overlap between the predicted segmentation and the ground truth whereas 1 indicates a perfect overlap between predicted segmentation and the ground truth.

Also, we augmented 600 (masks included) images to generate 1860 images from the second data set. The data set for training, validation, and testing were divided in the ratio of 7:2:1 respectively. We use the U-net model for biomedical image segmentation presented in [36]. All the implementation were performed using Keras [37]. To see the setting of the hyperparameters, performance training of the model, and visualization of the predicted masks see Additional file 1. The prediction was performed using the testing data set (not included in the training). The

predicted results are included in Tables 2 and 3. Other results obtained in other papers were also included for comparison.

We also present graphs in Figs. 10 and 11 to show the correlation of the size of the segmented area (nucleus and WBC) obtained using the proposed method and the ground truth.

The implementation of the proposed method was done by writing scripts in the python programming language, and it was run on a PC processor (Core i7-8650U CPU @ 1.90GHz \times 8). To process 40 images of 360×363 size, it takes 13.06518197059 seconds, which is approximately 0.326629549 seconds are used to process one image.

Discussion and conclusion

We propose a method for segmenting the nucleus and cytoplasm of the WBCs based on the local minima. The method estimates the threshold automatically from the input image by checking different conditions that allow a wide range of searching for a good approximation. The threshold is applied to the input image to segment the nucleus. The WBC is segmented and then the cytoplasm

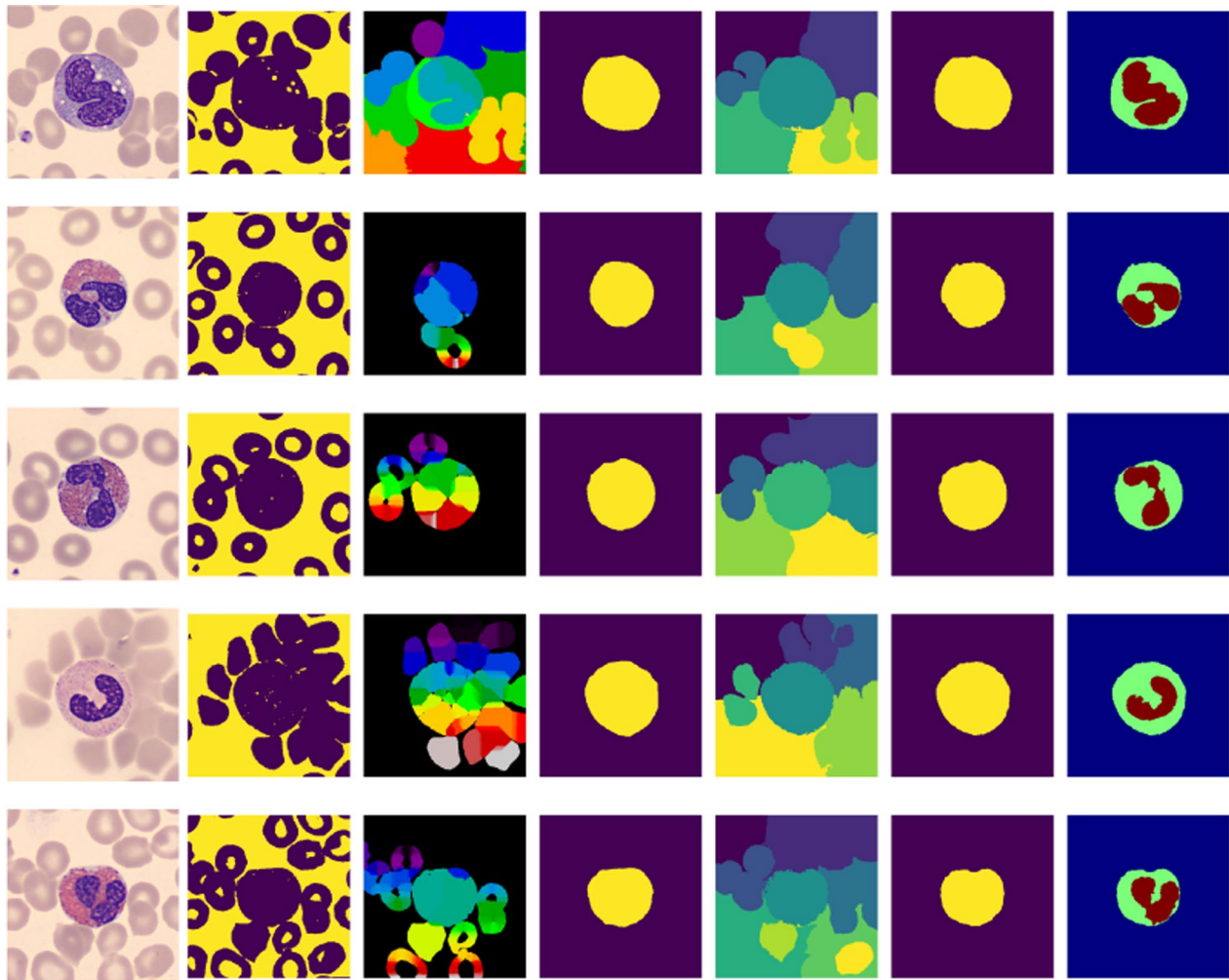


Fig. 8 WBC segmentation using SLIC and marker-controlled watershed. From the left, First column: input images, Second column: converted into grayscale and then binarized using the Otsu thresholding method. Third column: marker-controlled watershed segmentation using a distance transformation. Fourth column: Segmented WBC after post-processing the watershed results. Fifth column: segmentation of the input image using SLIC. Sixth column: Segmented WBC from SLIC results. Seventh column: Segmented nucleus and cytoplasm

is obtained by subtracting the segmented nucleus from the segmented WBC. The segmentation result is compared to ground truth to check the level of accuracy of the proposed method.

We segmented individual normal cells from the first data set which does not have ground truth. We also segmented images from the second dataset which has ground truth. The two data sets are significantly different from each other in terms of the colors of cytoplasm and background. But the results obtained from both data sets indicate that the proposed method can be applied to different image data sets. Figure 6 presents the results showing the nucleus segmentation steps whereas Fig. 7 presents the segmentation steps of cytoplasm and WBC. Figure 8 visualizes the results for cell segmentation using

SLIC and marker-controlled watershed. Table 1 gives a summary of the threshold and contrast means for the WBCs.

We provide a summary of the performance analysis of the proposed method. We use Jaccard indices, Dice similarity coefficients, sensitivity, specificity, and Precision to evaluate the performance of the proposed method. The performance analysis results are summarized in Tables 2 and 3. We also compare the result obtained using the proposed method to the state of art methods. Table 2 compares the performance of the method on segmenting nucleus to the results obtained using CNN, and SVM [21]. Table 3 compares the performance of the method on segmenting WBCs to the results obtained using a Deep neural network [22], U-Net [22] and WBC-Net [23].

Table 1 Summary for 976 sample images (251 eosinophils, 201 neutrophils, 208 monocytes, and 316 lymphocytes)

	Eosinophils	Neutrophils	Monocyte	Lymphocytes
Thresholds mean for Nucleus segmentation	0.338991314	0.356037820	0.359911376	0.362329243
Thresholds mean for WBC segmentation	0.894988532	0.887716863	0.892829014	0.890228957
Contrast Mean between nucleus and cytoplasm	0.555997217	0.531679043	0.532917638	0.527899714

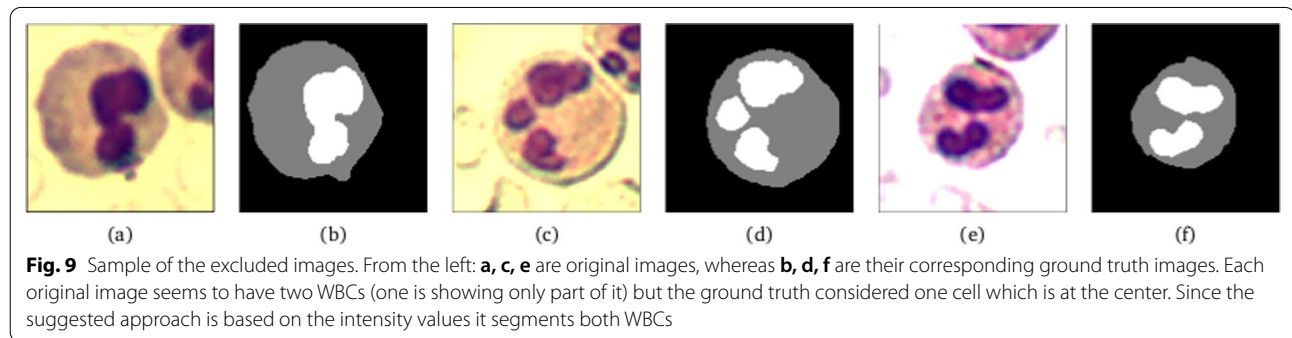


Table 2 The performance of the proposed method for nucleus segmentation compared to U-Net, CNN, support-vector machine (SVM) based on the data set two presented using average in each measure of similarity

	Jl	DSC	Specificity	Sensitivity	Precision
Proposed method	0.902925	0.948079	0.993110	0.952951	0.948903
U-Net [36]	0.917556	0.956456	0.995364	0.950505	0.964065
CNN [21]	-	0.910000	0.979200	0.960800	0.876300
SVM [21]	-	0.860000	0.818600	0.989700	0.934300

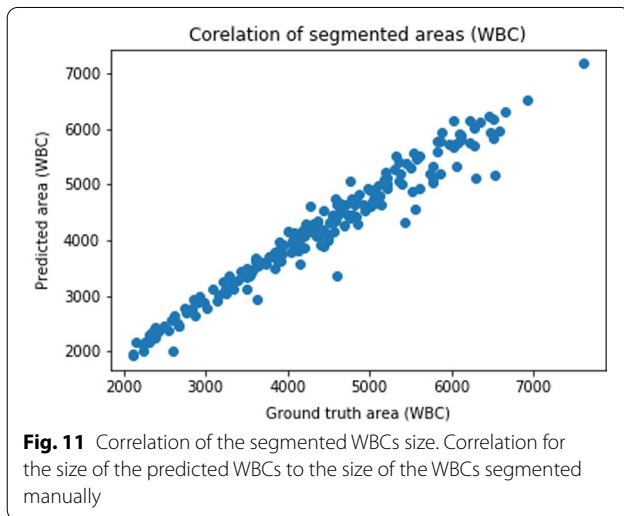
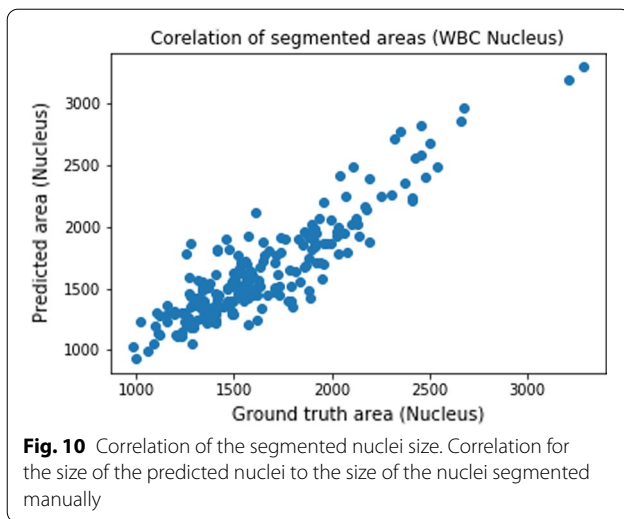
Also, we train the U-Net model in [36] on the augmented data and the results are included in Tables 2 and 3. Figure 10 provides a correlation of nuclei size between the predicted segmentation and the ground truth. Also, Fig. 11 gives a correlation of WBCs size between the predicted segmentation and the ground truth. Additional

file 1: Figs. 12 and 13 in present the convergence of the normalized forward sensitivity index.

We performed a visual representation of segmentation results obtained using the proposed method. We provide more segmentation results in Additional file 1: Figs. 14 to 17. Also, Additional file 1: Fig. 18 provides subgraphs showing the impact of the control parameters by tuning different values. Additional file 1: Figure 19 shows the training performance, Additional file 1: Figs. 20 and 21 shows the prediction of the nuclei and WBC masks respectively. The proposed method has demonstrated its effectiveness in segmenting high-quality and poor-quality images. For images in which the RBCs do not touch the WBCs, the method works well even if the cytoplasm color is indistinguishable from the RBC's color. For images in which the RBCs touch the WBCs, the method works well when the cytoplasm color is distinguishable from the RBCs.

Table 3 The performance of the proposed method for WBC segmentation compared to deep neural network (LeukocyteMask(Aug-ET)), U-Net (implemented in [22]) and WBC-Net based on the data set two presented using average in each measure of similarity

	Jl	DSC	Specificity	Sensitivity	Precision
Proposed method	0.942908	0.970176	0.975164	0.992475	0.950133
U-Net [36]	0.941467	0.969628	0.989037	0.962368	0.977735
Deep Neural Network [22]	-	0.981960	-	-	0.995440
U-Net [22]	-	0.961630	-	-	0.933190
WBC-Net [23]	-	0.989200	-	-	0.989700



Whenever the cytoplasm color is indistinguishable from the RBCs and they touch each other, techniques for separating touching objects can be used. For images with very low contrast between the cytoplasm and background, the method can successfully segment the nucleus, but not the cytoplasm.

Abbreviations

WBC: White blood cells; RBC: Red blood cells; SLIC: Simple linear iterative clustering; H and E: Hematoxylin and eosin; FCM: Fuzzy C- means algorithm; ALL: Acute lymphoblastic leukemia; RGB: Red, green, and blue; HSV: Hue saturation value; SVM: Support vector machine; ROI: Region of interest; JI: Jaccard index; DSC: Dice similarity coefficients; CIELAB: Implies $L^*a^*b^*$ color space, L^* for perceptual lightness, a^* and b^* for the four unique colors of human vision.

Supplementary Information

The online version contains supplementary material available at <https://doi.org/10.1186/s12880-022-00801-w>.

Additional file 1. The file presents sensitivity analysis of parameters, Fig. 14 to 18 present more experimental results. Also, the file presents briefly the concepts of B-Spline interpolation of the data points and the SLIC algorithm. Furthermore, the file presents results for the performance of the U-Net model training and the predicted masks for nuclei and WBCs.

Author contributions

SM implemented the proposed method and run the analysis to generate the results. JBH reviewed the biological concepts and clarity of the data set used. Interpretation of the results was done by all authors. Drafting, writing, and proofreading to approve the manuscript were done by all authors. All authors read and approved the final manuscript.

Funding

This research work is funded by the University of Bergen, Norway.

Availability of data and materials

All the data set analyzed in this study are freely available online. The first data set is available at "<https://data.mendeley.com/datasets/snk93bnjr/draft?a=d9582c71-9af0-4e59-9062-df30df05a121>" and the second data set is available at "<https://github.com/zxaoyou>".

Declarations

Competing interests

The authors declare that they have no competing interests.

Author details

¹Department of Mathematics, University of Bergen, Allégaten 41, 5007 Bergen, Norway. ²Department of Clinical Medicine, Neuro-SysMed, University of Bergen, PO box 7804, 5020 Bergen, Norway. ³Department of Neurology, Neuro-SysMed, Haukeland University Hospital, Jonas Lies vei 71, 5053 Bergen, Norway.

Received: 25 October 2021 Accepted: 12 April 2022

Published online: 26 April 2022

References

- Mathur A, Tripathi AS, Kuse M. Scalable system for classification of white blood cells from Leishman stained blood stain images. *J Pathol Inform.* 2013;4(Suppl):S15.
- Prinyakupt J, Pluempitwiriyaewej C. Segmentation of white blood cells and comparison of cell morphology by linear and Naïve Bayes classifiers. *Biomed Eng.* 2015;14(1):63.
- Hemalatha R, Thamizhvani T, Dhivya AJA, Joseph JE, Babu B, Chandrasekaran R. Active contour based segmentation techniques for medical image analysis. *Med Biol Image Anal.* 2018;17.
- Gonzalez RC, Woods RE. *Digital image processing*, 4th edn. 330 Hudson Street, New York, NY 10013;2008.
- Ismail A, Marhaban M. A simple approach to determine the best threshold value for automatic image thresholding. In: 2009 IEEE international conference on signal and image processing applications, pp. 162–6 (2009). IEEE.
- Lazar M, Hladnik A. Implementation of global and local thresholding algorithms in image segmentation of coloured prints. In: 35th international research conference IARIGAI, vol. 35 (2008).
- Singh TR, Roy S, Singh OI, Sinam T, Singh K, et al. A new local adaptive thresholding technique in binarization. *arXiv preprint arXiv:1201.5227* (2012).

8. Firdousi R, Parveen S. Local thresholding techniques in image binarization. *Int J Eng Comput Sci*. 2014;3(03):54.
9. Li Y, Zhu R, Mi L, Cao Y, Yao D. Segmentation of white blood cell from acute lymphoblastic leukemia images using dual-threshold method. *Comput Math Methods Med*. 2016;2016.
10. Chan Y-K, Tsai M-H, Huang D-C, Zheng Z-H, Hung K-D. Leukocyte nucleus segmentation and nucleus lobe counting. *BMC Bioinform*. 2010;11(1):1–18.
11. Theera-Umpon N. White blood cell segmentation and classification in microscopic bone marrow images. In: *International conference on fuzzy systems and knowledge discovery*, pp. 787–796 (2005). Springer.
12. Felzenszwalb PF, Huttenlocher DP. Efficient graph-based image segmentation. *Int J Comput Vis*. 2004;59(2):167–81.
13. Shi J, Malik J. Normalized cuts and image segmentation. In: *Proceedings of IEEE computer society conference on computer vision and pattern recognition*, pp. 731–737 (1997). IEEE.
14. Shi J, Malik J. Normalized cuts and image segmentation. *IEEE Trans Pattern Anal Mach Intell*. 2000;22(8):888–905.
15. Salem NM. Segmentation of white blood cells from microscopic images using k-means clustering. In: *2014 31st national radio science conference (NRSC)*, pp. 371–376 (2014). IEEE.
16. Miao H, Xiao C. Simultaneous segmentation of leukocyte and erythrocyte in microscopic images using a marker-controlled watershed algorithm. *Comput Math Methods Med*. 2018;2018.
17. Al-Dulaimi K, Tomeo-Reyes I, Banks J, Chandran V. White blood cell nuclei segmentation using level set methods and geometric active contours. In: *2016 international conference on digital image computing: techniques and applications (DICTA)*, pp. 1–7 (2016). IEEE.
18. Ghane N, Vard A, Talebi A, Nematollahy P. Segmentation of white blood cells from microscopic images using a novel combination of k-means clustering and modified watershed algorithm. *J Med Signals Sens*. 2017;7(2):92.
19. Kuse M, Sharma T, Gupta S. A classification scheme for lymphocyte segmentation in h&e stained histology images. In: *International conference on pattern recognition*, pp. 235–243 (2010). Springer.
20. Sadeghian F, Seman Z, Ramli AR, Kahar BHA, Saripan M-I. A framework for white blood cell segmentation in microscopic blood images using digital image processing. *Biol Proced*. 2009;11(1):196.
21. Banik PP, Saha R, Kim K-D. An automatic nucleus segmentation and CNN model based classification method of white blood cell. *Expert Syst Appl*. 2020;149:113211.
22. Fan H, Zhang F, Xi L, Li Z, Liu G, Xu Y. Leukocytemask: an automated localization and segmentation method for leukocyte in blood smear images using deep neural networks. *J Biophotonics*. 2019;12(7):201800488.
23. Lu Y, Qin X, Fan H, Lai T, Li Z. Wbc-net: a white blood cell segmentation network based on unet++ and resnet. *Appl Soft Comput*. 2021;101:107006.
24. Mittal A, Dhalla S, Gupta S, Gupta A. Automated analysis of blood smear images for leukemia detection: a comprehensive review. *ACM Comput Surv (CSUR)* (2022).
25. Long F. Microscopy cell nuclei segmentation with enhanced u-net. *BMC Bioinform*. 2020;21(1):1–12.
26. Achanta R, Shaji A, Smith K, Lucchi A, Fua P, Süsstrunk S. Slic superpixels compared to state-of-the-art superpixel methods. *IEEE Trans Pattern Anal Mach Intell*. 2012;34(11):2274–82.
27. Beucher S, et al. The watershed transformation applied to image segmentation. *Scan Microsc Suppl*. 1992;299.
28. Prautzsch H, Boehm W, Paluszny M. Bézier and B-spline techniques, vol. 6. Berlin: Springer; 2002.
29. Lyche T, Morken K. Spline methods draft. Oslo: Department of Informatics, Center of Mathematics for Applications, University of Oslo; 2008. p. 3–8.
30. Acevedo A, Merino A, Alférez S, Molina Á, Boldú L, Rodellar J. A dataset of microscopic peripheral blood cell images for development of automatic recognition systems. *Data Brief*. 2020;105474.
31. Zheng X, Wang Y, Wang G, Liu J. Fast and robust segmentation of white blood cell images by self-supervised learning. *Micron* 107.
32. ...Harris CR, Millman KJ, van der Walt SJ, Gommers R, Virtanen P, Cournapeau D, Wieser E, Taylor J, Berg S, Smith NJ, Kern R, Picus M, Hoyer S, van Kerkwijk MH, Brett M, Haldane A, Fernández del Río J, Wiebe M, Peterson P, Gérard-Marchant P, Sheppard K, Reddy T, Weckesser W, Abbas H, Gohlke C, Oliphant TE. Array programming with NumPy. *Nature*. 2020;585:357–62. <https://doi.org/10.1038/s41586-020-2649-2>.
33. ...Virtanen P, Gommers R, Oliphant TE, Haberland M, Reddy T, Cournapeau D, Burovski E, Peterson P, Weckesser W, Bright J, van der Walt SJ, Brett M, Wilson J, Millman KJ, Mayorov N, Nelson ARJ, Jones E, Kern R, Larson E, Carey CJ, Polat I, Feng Y, Moore EW, VanderPlas J, Laxalde D, Perktold J, Cimman R, Henriksen I, Quintero EA, Harris CR, Archibald AM, Ribeiro AH, Pedregosa F, van Mulbregt P. SciPy 1.0 contributors: SciPy 1.0: fundamental algorithms for scientific computing in python. *Nat Methods*. 2020;17:261–72. <https://doi.org/10.1038/s41592-019-0686-2>.
34. Liao P-S, Chen T-S, Chung P-C, et al. A fast algorithm for multilevel thresholding. *J Inf Sci Eng*. 2001;17(5):713–27.
35. Stutz D, Hermans A, Leibe B. Superpixels: an evaluation of the state-of-the-art. *Comput Vis Image Underst*. 2018;166:1–27.
36. Ronneberger O, Fischer P, Brox T. U-net: convolutional networks for biomedical image segmentation. In: *International conference on medical image computing and computer-assisted intervention*, pp. 234–241 (2015). Springer.
37. Chollet F, et al. Keras. <https://github.com/fchollet/keras>.

Publisher's Note

Springer Nature remains neutral with regard to jurisdictional claims in published maps and institutional affiliations.

Ready to submit your research? Choose BMC and benefit from:

- fast, convenient online submission
- thorough peer review by experienced researchers in your field
- rapid publication on acceptance
- support for research data, including large and complex data types
- gold Open Access which fosters wider collaboration and increased citations
- maximum visibility for your research: over 100M website views per year

At BMC, research is always in progress.

Learn more biomedcentral.com/submissions

